Dalton Transactions

ROYAL SOCIETY OF CHEMISTRY

PAPER

View Article Online
View Journal | View Issue



Cite this: *Dalton Trans.*, 2021, **50**, 16099

# Are lanthanide-transition metal direct bonds a route to achieving new generation {3d–4f} SMMs?†

Abinash Swain, Asmita Sen and Gopalan Rajaraman *

Lanthanide based single-molecule magnets are gaining wide attention due to their potential applications in emerging technologies. One of the main challenges in this area is quenching quantum tunnelling of magnetisation (QTM), which often undercuts the magnetisation reversal barrier. Among the several strategies employed, enhancing exchange coupling has been studied in detail, with large exchanges resulting in stronger quenching of QTM effects. Lanthanides, however, suffer from weak exchanges offered by the deeply buried 4f orbitals and the numerous attempts to enhance the exchange coupling in the {3d–4f} pairs have not exceeded values larger than 30 $cm^{-1}$. In this work, using a combination of DFT and the *ab initio* CASSCF/RASSI-SO method, we have explored lanthanide-transition metal direct bonds as a tool to quench QTM effects. In this direction, we have modelled $[PyCp_2LnMCp(CO)_2]$ (Ln = Gd(III), Dy(III), and Er(III) and M = V(0), Mn(0), Co(0) and Fe(I) and here $PyCp_2$ = $[2,6\text{-}(CH_2C_5H_3)_2C_5H_3N]_2^-$ using $[PyCp_2DyFeCp(CO)_2]$ as an example as reported by Nippe *et al.* (C. P. Burns, X. Yang, J. D. Wofford, N. S. Bhuvanesh, M. B. Hall and M. Nippe, *Angew. Chem., Int. Ed.* 2018, **57**, 8144). Bonding analysis reveals a dative Ln–TM bond with a donation of $\pi(V/Mnd_{xy}–\pi^*CO)$ to $5d_{z^2}$ (Gd) in the case of Gd–V and Gd–Mn and 4s(Co) to $5d_{xy}/5d_{yz}$ (Gd) for Gd–Co with the transition metal ion being found in the low-spin $S = \frac{1}{2}$ configurations in all the cases. B3LYP/TZV (Gd;CSDZ) calculations on $[PyCp_2GdMCp(CO)_2]$ yield $J_{Gd-V}$ = −46.1 $cm^{-1}$, $J_{Gd-Mn}$ = −57.1 $cm^{-1}$, $J_{Gd-Co}$ = +55.3 $cm^{-1}$, $J_{Gd-Fe^+}$ = +13.9 $cm^{-1}$, $J_{Gd-Vhs}$ = −162.1 $cm^{-1}$ and $J_{Gd-Mnhs}$ = −343.9 $cm^{-1}$ and unveiling record-high $J$ values for {3d–4f} complexes. The mechanism of magnetic coupling is developed, which discloses the dominating presence of strong 3d–4f orbital overlaps in most of the cases studied, leading to antiferromagnetic exchange. When these overlaps are weaker and 3d to $Gd(5d_{z^2})$, charge transfer dominates, yielding a ferromagnetic coupling for the Gd–Co/Gd–$Fe^+$ complexes. Calculations performed on the anisotropic Dy(III) and Er(III) complexes reveal that the ground state $g_{zz}$ axis lies along the Cp–Ln–Cp axis and the Ln–TM bonds, respectively. Thus the Ln–TM bond hinders the single-ion anisotropy of Dy(III) by offering equatorial ligation and lowering the $m_J = \pm\frac{1}{2}$ state energy, and at the same time, helping in enhancing the axiality of Er(III). When strong {3d–4f} exchange couplings are introduced, record-high barrier heights as high as 229 $cm^{-1}$ were accomplished. Furthermore, the exchange coupling annihilates the QTM effects and suggests the lanthanide-transition metal direct bond as a viable alternative to enhance exchange coupling to bring {3d–4f} complexes back in the race for high-blocking SMMs.

Received 7th July 2021,
Accepted 27th September 2021

DOI: 10.1039/d1dt02256c

rsc.li/dalton

## Introduction

Single-molecule magnets[1] have attracted wide attention in recent years due to their potential applications proposed in various emerging technologies such as solid-state hard discs based on individual molecules, Q-bits for quantum computing and molecular spintronics devices to name a few.[2–6] As various applications demand different magnetic characteristics, it is important to find a viable way to control the microscopic spin Hamiltonian parameters associated with these molecules to accomplish the potential applications proposed.[7] For information storage devices, attaining a large barrier height for magnetisation reversal ($U_{eff}$) and a large blocking temperature ($T_B$) below which the magnetisation is fully frozen are vital.[8] In addition, quenching the quantum tunnelling of magnetisation (QTM)[9] is also crucial for further developments. Recently, dys-

*Department of Chemistry, Indian Institute of Technology Bombay, Powai, Mumbai – 400076, India. E-mail: rajaraman@chem.iitb.ac.in*

†Electronic supplementary information (ESI) available: NBO plots, *ab initio* results, and DFT optimised structures along with corresponding coordinates. See DOI: 10.1039/d1dt02256c

procenium motif-containing single-ion magnets (SIMs) have been reported with a very large blocking temperature in the range of 60–80 K.[10,11] Despite such large blocking temperatures, these molecules also show QTM features at zero-field, which is perhaps common for most of the single-ion magnets reported. Among others, an effective way of quenching zero-field QTM lies in inducing strong exchange coupling in these systems.[12] However, as lanthanide 4f-orbitals are deeply buried, they interact feebly with ligands offering very weak super-exchange in 4f–4f complexes (0 to 1 $cm^{-1}$), weak super-exchange in 3d–4f systems (0 to 10 $cm^{-1}$) and moderate direct-exchange in radical-4f complexes (1 to 30 $cm^{-1}$).[13–15]

Many strategies to enhance exchange coupling in these systems are developed and include (i) fine-tuning the bridging atoms such as oxygen, halides, nitrogen *etc.*[15–18,19] (ii) employing radical ligands such as $N_2^{3-}$ as bridging ligands,[20,21] (iii) utilising soft donor atoms such as sulphur to enhance delocalization,[22] and (iv) employing 4d-elements possessing much larger diffused-orbitals.[23] This has resulted in an array of SMMs with attractive $U_{eff}$ values with significantly diminished zero-field QTM. This includes (a) $\{TM_2Dy_2\}$[24] (TM = 3d or 4d) SMMs exhibiting $U_{eff}$ values in the range of 3.5 $cm^{-1}$ to 87 $cm^{-1}$, (b) $\{Ln_2N_2^{3-}\}$ SMMs exhibiting $U_{eff}$ values of 227 $cm^{-1}$ with attractive $T_B$ values (14 K),[20] (c) unconventional lanthanide encapsulated fullerenes such as $Dy_2@C_{80}Ph$ and $Tb_2/Dy_2@C_{79}N$ exhibiting large $U_{eff}$ and $T_B$ values (426 to 757$cm^{-1}$ and 21 K to 24 K) unveiled based on earlier predictions,[25,26] and (d) $\{Fe_2Dy\}$ SMMs exhibiting a $U_{eff}$ value of 416 $cm^{-1}$.[27]

Despite several attempts, exchange coupling in conventional coordination/organometallic compounds remains moderate in the order of ~30 $cm^{-1}$ in 4f-radical systems and much smaller in {3d–4f} systems. Our group has also studied in the past various combinations of {3d–4f} and {radical-4f} systems and developed several magnetostructural correlations to enhance exchange coupling. Nevertheless, the predicted range of $J$ lies within 30–40 $cm^{-1}$.[28–30] The established mechanism of magnetic exchange in {3d–4f} and {radical-4f} systems reveal the participation of the empty 5d/6s orbital of 4f ions in charge transfer which often resulted in weak ferromagnetic exchanges. To obtain a very strong exchange that is much larger in magnitude, it is important to induce interaction between the 4f orbitals and 3d orbitals directly. This is possible only if a direct metal–metal bond between 4f and 3d metals is enabled. The first demonstration of this kind emerged from the work of Beletskaya *et al.* in 1993 who reported unsupported Ln–TM bond in $[Cp_2(thf)Lu\text{-}RuCp(CO)_2]$ with a Lu–Ru direct metal–metal bond.[31] Later on, this was further developed by Arnold *et al.*, who have reported an unsupported Ln–Fe complex, $[(L')(N'')Nd\text{–}FeCp(CO)_2]_2$ [L′ = $ButNCH_2CH_2\{C\text{-}(NCSiMe_3CHNBut)\}$; N″ = $N(SiMe_3)_2$] with a Nd–Fe X-ray structure reported with the metal–metal bond distance of 2.994 Å.[32] Later, several bismetallocene $[Cp_2Ln\text{–}ReCp_2]$ type complexes were reported with unsupported Ln–Re bonds.[33–35] However, magnetic studies were not reported in any of these systems. In this regard, the report by Nippe *et al.*[36] on $[PyCp_2LnMCp(CO)_2]$ (Ln = Dy and M = Fe and Ru and here $PyCp_2 = [2,6\text{-}(CH_2C_5H_3)_2C_5H_3N]_2^-$ shows Fig. 1) that complexes with the first Dy–Fe and Dy–Ru metal–metal direct bonds gain attention as these are the first of this class of molecules to show slow magnetic relaxation with the Dy–Fe bond exhibiting a $U_{eff}$ value of 40 $cm^{-1}$ and the Dy–Ru bond 36 $cm^{-1}$, albeit in the presence of an applied magnetic field.[36] In these complexes, the lanthanide ion is in a +3 oxidation state, whereas the transition metal is zero-valent and hence diamagnetic. Despite the advantage of having the desired 4f–3d bonds, the diamagnetic characteristic of the transition metal ion does not help in achieving the desired magnetic characteristic *via* exchange-induced QTM quenching as mentioned above. It is also important to note that if a large $U_{eff}$ is achieved with very strong exchange coupling, which can quench the QTM effects, it is expected to yield SMMs with attractive blocking temperatures.

Theoretical calculations based on density functional theory (DFT) and *ab initio* (CASSCF) calculations played a proactive role in the design and development of molecular magnets over

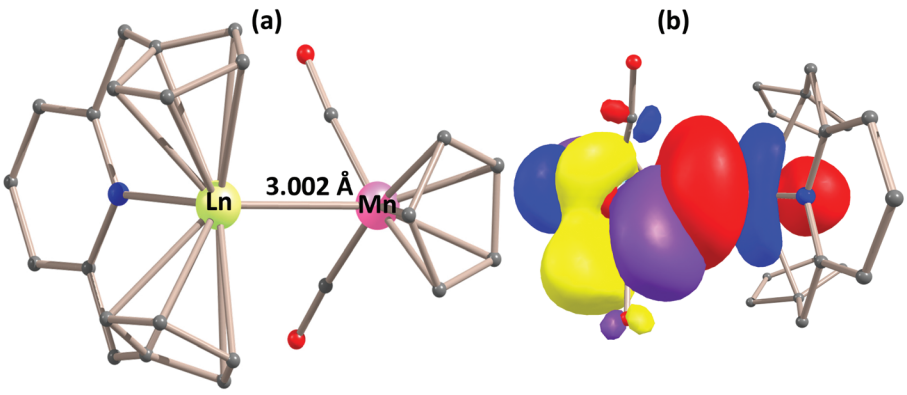


**Fig. 1** (a) DFT optimised structure of **Gd–Mn** and here Ln–V = 3.191 Å, Ln–Co = 2.792 Å, Ln–Fe = 3.457 Å, Ln–$V_{hs}$ = 3.495 Å and Ln–$Mn_{hs}$ = 3.328 Å. Yellow = Ln, pink = Mn, grey = C, red = O, and blue = N. Hydrogen atoms are omitted for clarity. (b) NBO computed donor–acceptor interaction corresponding to the Gd–V bond involving (V-$d_{x^2-y^2}$–π*CO) → $5d_{xy}$ (Gd) donation.

 

the decades.[7,37–39] Over the years, these methods are not only used to rationalise the experimental observations but also to make robust predictions to guide experimentalists. In this work, we have employed DFT and CASSCF calculations to study paramagnetic 3d metal ions in $[PyCp_2LnMCp(CO)_2]$ (Ln = Gd(III), Dy(III), and Er(III) and M = V(0), Mn(0), Fe(I), and Co (0), and $PyCp_2$ = $[2,6\text{-}(CH_2C_5H_3)_2C_5H_3N]_2^-$) complexes to understand the sign and strength of magnetic exchange that arises due to such 3d–4f metal–metal bonds. In particular, our work aims to answer the following intriguing questions in this area (i) how large should the 3d–4f exchange be in such metal–metal bonded systems? (ii) what is the mechanism of magnetic exchange that operates between the two metal ions? and (iii) does the computed exchange translate to a larger effective energy barrier for the anisotropic lanthanide ions?

## Computational methodologies

All the calculations were performed on modelled structures derived from the reported **Dy–Fe** X-ray structure.[36] The structures were optimised using density functional methods with the G16 suite of programs.[40] All optimised structures were determined to mimina with no negative frequencies with the exception of **Dy–V** where a small negative frequency of ~80 $cm^{-1}$ detected. This frequency corresponds to a distance alkyl rotations and our attempts to eliminate this frequency has not succeded. The Dy ion was replaced by Y for structural optimisation by employing the B3LYP-D3 functional at the TZVP level of basis set for Y, 6-311 g(d,p) for the transition metal ion and 6-31G* for the rest of the atoms.[41,42] The Y ion is replaced by Gd(III) ion for the calculation of exchange interaction, *J*. For the single point energy calculations to derive the exchange parameters, the CSDZ basis set was used for Gd(III) ion and Ahlrich's TZV basis set was used for the rest of the atoms.[43–45] The transition metal ion in all the cases studied has the $S = \frac{1}{2}$ state (*vide infra*). As an isotropic exchange interaction has been employed here, the orbital degeneracy on the transition metal ion needs to be ruled out. To crosscheck this, we performed SA-CASSCF calculations using the ORCA 4.2.1 suite.[46,47] These calculations were then analysed and the AILFT[48] d-based orbitals were plotted, which suggested that the low lying d orbitals are well separated from each other (by more than 3000 $cm^{-1}$). The ligand field here quenches the first-order orbital degeneracy of the transition metal atom to enable us to treat them as an isotropic $S = \frac{1}{2}$ system. For anisotropic lanthanide systems, *ab initio* calculations were performed using the MOLCAS 8.0[49] package by employing the CASSCF/RASSI-SO/SINGLE-ANSIO/POLY-ANISO module to develop the mechanism of slow relaxation of magnetisation.[50–54] The *ab initio* calculations were performed on the Dy and Er analogues of the optimised complexes where Y was replaced with the corresponding paramagnetic metal ions to derive the magnetic properties. For the Ln = Dy(III) and Er(III) and the transition metals, the ANO-RCC type TZVP level of basis set, for C the N TZV level, for O and H a DZV level basis sets were used.[55] The DKH Hamiltonian was employed to account for the relativistic effects.[56] For the Dy(III) ion, only 21 sextet roots were considered for all the systems with the exception of the **Dy–Mn** structure, for which all the all sextets, quartets and doublet roots were taken into account to assess the results (see Table S3 in the ESI†). This assessment reveals that the results are very similar, offering confidence in the choice of 21 sextet roots for the Dy(III) ion, thus reducing the computational cost significantly. For the Er(III) ion, 112 doublets and 35 quartets were employed. These roots were then mixed in RASSI-SO and the results were then utilised to compute the magnetic properties using the SINGLE_ANISO routine for monomeric models and the POLY_ANISO routine for the dimeric models.[55] NBO analysis was performed to understand the nature of the Ln–TM direct bond using the DFT computed wave function.[57] The DFT computed *J* values of the Gd–TM systems were further used in the *ab initio* methods to derive the overall magnetic blocking for the entire complex originating from the exchanged coupled state using the Lines model in the POLY_ANISO routine. The following Hamiltonian was employed for the exchange calculations using the broken symmetry approach.[58,59,60]

$$\hat{H} = -2J\hat{S}_{Gd}\hat{S}_{M}$$

where, $S_{Gd}$ = spin of Gd and $S_M$ = spin of the transition metal. For the complex Gd–TM {TM = V, Mn, Co, and $Fe^+$}, the calculations were performed in a high spin state ($S = 4$) and a broken symmetry spin state ($S = 3$).[61,62] The transition metal was found to inherit a low-spin configuration due to the strong ligand field exerted by the CO and Cp rings with the following d-electronic configurations V(0) – $(d_{yz})^2(d_{xz})^2(d_{xy})^1(d_{z^2})^0(d_{x^2-y^2})^0$; Mn(0) – $(d_{yz})^2(d_{xz})^2(d_{xy})^2(d_{z^2})^1(d_{x^2-y^2})^0$; Co(0) – $(d_{yz})^2(d_{xz})^2(d_{xy})^2(d_{z^2})^2(d_{x^2-y^2})^1$; and Fe(I) – $(d_{yz})^2(d_{xz})^2(d_{xy})^2(d_{z^2})^1(d_{x^2-y^2})^0$. In addition, we also considered the high-spin excited states for V and Mn with the electronic configuration of V(0) – $(d_{yz})^1(d_{xz})^1(d_{xy})^1(d_{z^2})^1(d_{x^2-y^2})^1$ and Mn(0) – $(d_{yz})^2(d_{xz})^2(d_{xy})^1(d_{z^2})^1(d_{x^2-y^2})^1$. The high-spin nature of the transition metal ion is denoted in the subscript; for example, **Gd–$V_{hs}$** suggests V(0) in the high-spin state. The respective energy differences between the high and low spin states are provided in Table S1.†

## Results and discussion

### Structure and bonding of Gd–V, Gd–Mn, Gd–Co and Gd–$Fe^+$ complexes

The DFT calculated geometries of the **Gd–V**, **Gd–Mn**, **Gd–Co** and **Gd–$Fe^+$** complexes are shown in Fig. 1 and the selected structural parameters are given in Table 1. Our calculations performed on the **Ln–Fe** geometry reproduces the X-ray structure with the **Dy–Fe** distance of 2.850 Å compared to 2.880 Å reported (see Table 1), offering confidence in the chosen methodology. The Gd–TM bond lengths were found to vary from 2.790 Å (**Gd–Co**) to 3.495 Å (**Gd–$V_{hs}$**) in the following order **Gd–Co** < **Gd–Mn** < **Gd–V** < **Gd–$Mn_{hs}$** < **Gd–$Fe^+$** < **Gd–$V_{hs}$**. Among the low-spin complexes, the trend suggests that Co(0) with the

Table 1 Computed exchange parameters, bond parameters, overlap integrals using density functional methodologies. The experimental bond parameters for **Dy–Fe** are reported in parenthesis

| Complexes | Gd–M (Å) | M–Gd–Cp/Cp–Gd–Cp (°) | $J_{exch}$ ($cm^{-1}$) | $^{total}S_{ij}(J_F,J_{AF})$ | Wieberg BE |
|---|---|---|---|---|---|
| Gd–V | 3.191 | 115.4/126 | −46.1 | 0.053 | 0.186 |
| Gd–Mn | 3.002 | 113.7/128.7 | −57.1 | 0.181 | 0.26 |
| Gd–Co | 2.792 | 114.1/129.3 | +55.3 | 0.009 | 0.304 |
| Gd–$Fe^+$ | 3.457 | 111.3/134.2 | +13.9 | — | — |
| Gd–V(hs) | 3.495 | 106.4/139.1 | −162.1 | 0.224 | — |
| Gd–Mn(hs) | 3.328 | 111.4/135.2 | −343.9 | 0.792 | — |
| Gd–Fe | 2.850 (2.883) | 113.6/126.6 (113.2/130.9) | — | | 0.122 |

$(d_{yz})^2(d_{xz})^2(d_{xy})^2(d_{z^2})^2(d_{x^2-y^2})^1$ electronic configuration is a stronger donor, and this is attributed to the fully occupied d-orbitals making a stronger donation. Depleting the electron density from the $d_{z^2}$ orbital reduces the TM → Gd(III) donation leading to longer Ln–TM bonds in the **Gd–Mn** complex. Reducing the d-electron density further in V(0) elongates the bond even further (by ∼0.4 Å). Among these complexes, V and Mn with the high-spin $S$ = 5/2 and $S$ = 3/2 states were found to have much longer Ln–TM bond lengths as the spin-down β-electron densities are depleted here. **Gd–$Fe^+$**, as expected, has much longer Ln–TM bond lengths compared to the **Gd–Fe** compound (larger by ∼0.6 Å). We have analysed various bond angles (see Table 1), and only minor alterations in the angles are noted among the series. Furthermore, Wieberg bond indices (see Table 1) suggest a direct interaction between the transition metal and lanthanide ion, with a WBI index of 0.186 for **Gd–V** and 0.304 for **Gd–Co**. The WBI of **Gd–Co** is the largest value computed, reflecting the metal–metal distance trend. It is important to note here that these values are shorter than those required for covalent or coordinate-covalent bonds and are in the range of $BH_3$→$NH_3$ dative bonds.[63] We have also looked at the density matrix between the two centres which indicates the presence of a substantial interaction. This is also exemplified by the QTAIM analysis performed wherein $\nabla^2\rho(_{lcp})$ in the range of 0.043–0.039 are obtained, suggesting stronger interactions (see Table S4†). Recently, Nippe *et al.* reported the structure and bonding of the **Dy–Fe** complex[64] and have shown that there is a dative bond formation between the Fe and Dy ions. To understand this Ln–TM bond further, they have substituted the transition metal ions with Ca and Zn, thus unveiling the ionic nature of the Ln–TM bond with shorter bond lengths leading to stronger donation with enhanced covalent contributions. Our results are in agreement with their reports on the **Dy–Fe** complex.

We performed an NBO analysis to understand the nature of the Ln–TM bond in the example studied. In the **Gd–V** complex, there are several donor–acceptor interactions between the V and Gd atoms, with the most prominent one being the 4s(V) → $5d_{xy}$/$5d_{z^2}$ (Gd) interaction (Fig. 1b; 174.8 kcal $mol^{-1}$, 36.3 kcal $mol^{-1}$, 11.9 kcal $mol^{-1}$) followed by the weaker π($V\text{-}d_{x^2-y^2}$–π*CO) → $5d_{xy}$ (Gd) (11.0 kcal $mol^{-1}$) interaction (Fig. S6a†). The second interaction BD(V–C) consists of the valence $3d_{x^2-y^2}$ orbital of V and the π* orbital of CO, which is donating an electron to the vacant $5d_{xy}$ orbital of Gd. In the V–C donor, the V is $sp^{0.68}d^{99.99}$ hybridised while the C(O) is in $sp^{91.24}$ hybridisation. A similar kind of bonding is present in the **Gd–Mn** complex, with π(Mn-$d_{xz}$–π*CO) → $5d_{xy}$ (Gd) (18.4 kcal $mol^{-1}$) and a back donation involving the same metal orbitals (209.3 kcal $mol^{-1}$; Fig. S6b†). In both the Mn–C bonding, Mn is $sd^{1.21}$ hybridised while CO is $sp^{0.54}$. The $sd^{1.21}$ hybridisation involves the 4s and $3d_{xz}$ orbitals of Mn. In the **Gd–Co** complex, a combination of donor–acceptor interactions is noticed involving the $5d_{z^2}$/$5d_{xy}$ (Lp*) orbital and the 4s (Lp*) orbitals of Gd and Co ions, respectively. A retro-dative type of interaction where 4s(Co) → $5d_{xy}$ Lp*(Gd) (43.9 kcal $mol^{-1}$) and a back donation of $5d_{z^2}$ (Gd) → 4s(Co) (171.7 and 200.1 kcal $mol^{-1}$) were observed (Fig. S6c†). For **Gd–Fe**, a one electron (∼0.754) 2-centred bond between Gd and Fe centres is detected with the $3d_{z^2}$ orbital of Fe and $5d_{z^2}$ orbital of Gd involved. The Fe centre is found to be $sd^{9.71}$ hybridised and the Gd centre is $sp^{1.4}d^{2.02}$ hybridised. This bond is extremely ionic, with the electron density near the Fe centre, present in the $Gd^+Fe^-$ form.

The transition metal ion in these complexes is coordinated to three strong field ligands and hence are expected to stabilise low-spin configurations.[65] For **Gd–V** and **Gd–Mn**, we have also optimized the corresponding high-spin configuration (V(0) – $(d_{yz})^1(d_{xz})^1(d_{xy})^1(d_{z^2})^1(d_{x^2-y^2})^1$ and Mn(0) – $(d_{yz})^2(d_{xz})^2(d_{xy})^1(d_{z^2})^1(d_{x^2-y^2})^1$) for transition metal ions, *i.e.* the $S_V$ = 5/2 and $S_{Mn}$ = 3/2 states and these were found to be 25 kcal $mol^{-1}$ and 42 kcal $mol^{-1}$ higher in energy (Table S1†) from the corresponding low-spin $S_{V,\ Mn}$ = 1/2 configurations. This is in line with the expected ligand field theory and the high-spin state in the **Gd–V** is relatively small and suggests a possibility of accessing them *via* photoexcitations. As the zero-valent low-spin configurations of the transition metal ions shown here may exhibit orbital degeneracy, this would void the application of DFT calculations of isotropic *J*s. To check this possibility, we performed SA-CASSCF calculations on all the transition metal ions studied and the corresponding AILFT orbitals are shown in Fig. 2. For the **Gd–V** complex, the AILFT calculations reveal that an unpaired electron resides in the $d_{xy}$ orbital with the orbital splitting ($\Delta(Ed_{yz} - Ed_{xy})$) exceeding 8437 $cm^{-1}$(Fig. 2a), thus ruling out the possibility of strong orbital degeneracy. In particular, the $d_{yz}$ orbital is stabilised significantly compared to the $d_{xz}$ and $d_{xy}$ orbitals. The $d_{yz}$ orbital lies on the plane of the two CO ligands and hence stronger π-donations to this orbital lead to a greater stabilis-

 

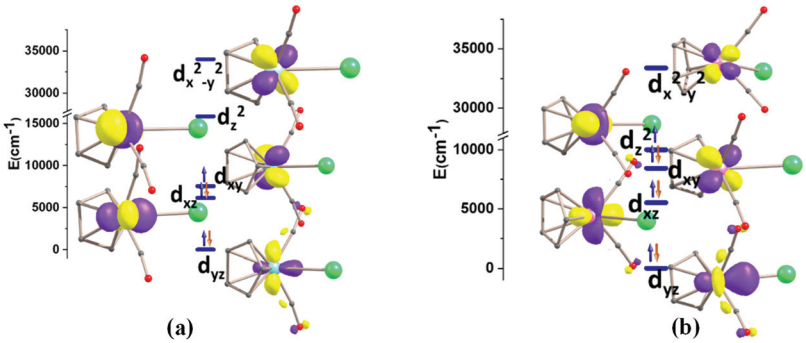


Fig. 2 Eigen value plot for the d orbital splitting for complex **Ln–V** (a) and **Ln–Mn** (b) obtained by AILFT approach.

ation. This is followed by the $d_{xz}$ orbital that lies in the direction of the Cp ring and then by the $d_{xy}$ orbital that exhibits δ-type interaction with the ligands. For **Gd–Mn** (see Fig. 2b), the AILFT calculations suggest that the unpaired electron located in the $d_{z^2}$ orbital follows a similar pattern with the orbital splitting ($\Delta(Ed_{yz} - Ed_{z^2})$) exceeding 15 851 $cm^{-1}$ suggesting that asymmetric ligands lift the degeneracy and quench the orbital contributions that are generally common among the $S = \frac{1}{2}$ d-electronic configurations.[66] A similar scenario envisioned for other metal ions suggested that isotropic exchange coupling is a valid parameter for this system.

### Magnetic exchange and mechanism of magnetic coupling in the Gd–V, Gd–Mn, Gd–Co and Gd–$Fe^+$ complexes

The magnetic exchange $J$ computed using DFT calculations for the optimised geometries of **Gd–V**, **Gd–Mn**, **Gd–Co** and **Gd–$Fe^+$** are shown in Table 1. The calculations reveal a strong antiferromagnetic coupling of −46.1 $cm^{-1}$ for the **Gd–V** complex and −57.1 $cm^{-1}$ for the **Gd–Mn** complex while strong ferromagnetic couplings are noted for the **Gd–Co** (+55.3 $cm^{-1}$) and **Gd–$Fe^+$** (+13.9 $cm^{-1}$) complexes (Table 1). For the **Gd–$V_{hs}$** and **Gd–$Mn_{hs}$** systems, the computed $J$ values are antiferromagnetic in nature and are an order of magnitude larger (−162.1 $cm^{-1}$ and −343.9 $cm^{-1}$, see Table 1). These computed $J$ values are by far the largest exchange coupling known for any 3d–4f pairs suggesting an unusual but viable route to enhance the exchange coupling constants. The computed spin density plot of the broken symmetry solution is shown in Fig. 3 (ESI Fig. S1†). In all the cases, the Gd(III) ion was found to have a spin density above 7.0 that is expected based on spin polarisation, while the transition metal ion exhibited a mixture of lower (V, Co) and higher (Mn and $Fe^+$) spin densities due to delocalisation/polarisation. If the unpaired electron on the 3d metal ion is in the $3d_{z^2}$ orbital, it promotes stronger spin polarisation, while in all other cases, spin delocalisation is dominant. This is contrary to the expectation based on the octahedral ligand field.

While such large exchange couplings are unusual, it is important to note here that these are due to direct exchange and not super-exchange, which is usually responsible for magnetic coupling in {3d–4f} systems. Furthermore, if such direct exchanges are permitted, stronger exchanges as high as −27 $cm^{-1}$ are noted for $\{Gd_2N_2^{3-}\}$ complexes.[13,21] To understand the sign and strength of these $J$ values, the mechanism of magnetic coupling needs to be elucidated. The following points emerge from the mechanism of magnetic coupling developed based on DFT and *ab initio* CASSCF calculations over the years for the super-exchange interactions present in {3d-Gd} complexes:[67,68] (i) the antiferromagnetic part of the exchange arises solely from the overlap of SOMOs, (ii) there are two contributions to the ferromagnetic part of the exchange—the orthogonality between the SOMOs and the

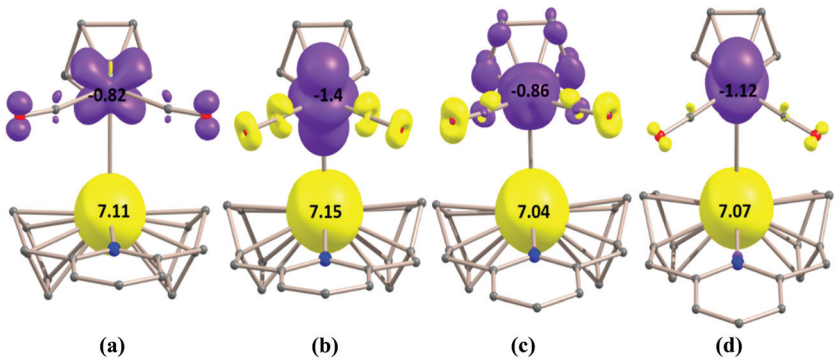


Fig. 3 DFT computed spin density plots for (a) **Gd–V**, (b) **Gd–Mn**, (c) **Gd–Co**, and (d) **Gd–$Fe^+$**.

charge transfer from the 3d orbitals to the formally empty 5d orbitals of the Gd(III) ions and (iii) the charge transfer is generally larger if the unpaired electron in the 3d orbitals is present in σ type $d_{z^2}$ or $d_{x^2-y^2}$ orbitals rather than the $d_{xz}/d_{xz}/d_{yz}$ orbitals. While we can take a cue from the {3d-Gd} mechanism of magnetic coupling developed earlier,[28–30] due to the presence of direct exchange, various contributions should be analysed in detail. In particular, in {3d-Gd} complexes, the antiferromagnetic contribution is generally weak due to the feeble overlap of the 4f orbitals with the ligand, which in turn overlap with the 3d orbitals, leading to ferromagnetic coupling in the majority of the examples studied. The DFT Eigen-value plot of **Gd–V** is shown in Fig. 4a. Here the $4f^7$ orbitals are, as expected, deeply buried (>10 eV) from the frontier V-3d orbital while there are several MOs with a significant Gd(III) 5d character close to the V-3d orbitals. This clearly suggests that charge transfer from the V(3d) orbital to the Gd(4f) orbital is not possible, but stronger charger transfer to Gd(5d) orbitals are expected. Thus this charge transfer mechanism is different from the charge transfer mechanism well established in transition metal dimers as well as metal-superoxo species.[69] We would like to note that DFT calculations generally suffer from delocalisation errors, and the charge transfer contributions thus are generally overestimated. However, our earlier DFT and

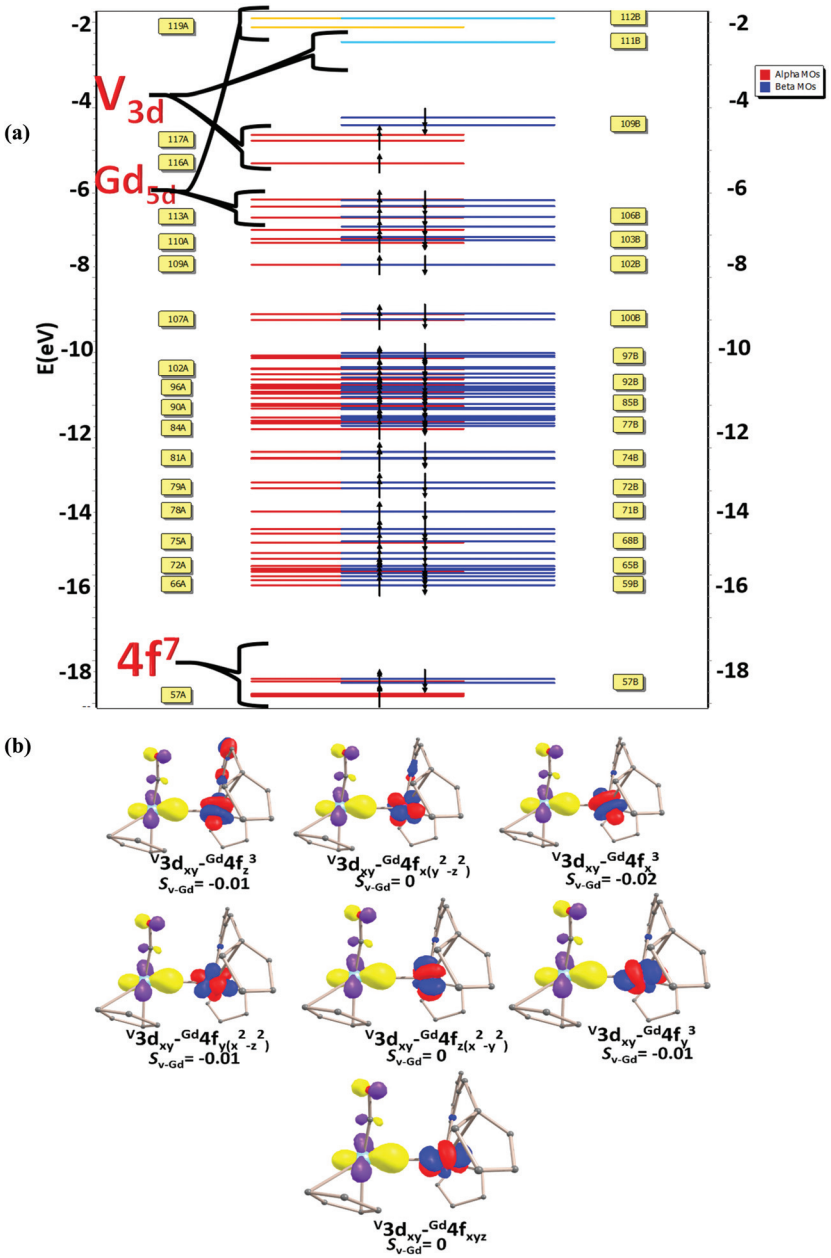


**Fig. 4** (a) Eigenvalue plot for **Gd–V** complex obtained from DFT calculations showing various orbitals and their relative energies. (b) The overlap between Gd-$4f^7$ and V-$3d_{xy}$ for **Gd–V** complex. $S_{V-Gd}$ represents the computed overlap integral.

 

*ab initio* CASSCF calculations on {V-Gd} dimers reveal that, while the charge transfer contributions are overestimated, DFT calculations, particularly the hybrid B3LYP functional employed, can reproduce both the sign and strength of the exchange coupling present in these systems, offering confidence on the $J$ values and their corresponding contributions.[30]

The dominant contribution between the overlap and the charge transfer decides the overall nature of the $J$ value. In general, for {3d–4f} super-exchange coupled dimers, the 3d–4f orbital overlaps are extremely weak, leading to a dominant $J_F$ term and hence a ferromagnetic coupling. However, there are examples of antiferromagnetically coupled {3d-Gd} pairs. In particular, the {V-Gd} pair studied by us earlier reveals an antiferromagnetic coupling arising due to the strong overlap between the $3d_{xy}$ and $4f_{xyz}$ orbitals. However, the exchange noted is very weak ($J_{cal} = -0.7$ cm$^{-1}$ and $J_{exp} = -2.6$ cm$^{-1}$).[30] To assess the antiferromagnetic contribution to the exchange, we computed the overlap integral between the SOMOs (see Table S2a–S2c in ESI†). Several significant overlaps are detected with a dominant $3d_{xy}$–$4f_{x^3}$ overlap for the Gd–V complex, as shown in Fig. 4b. As the $3d_{xy}$ orbital lobe is pointing towards the Gd–V bond, 4f orbitals having a nodal plane along the bond have zero overlaps. Our calculations reveal four strong overlaps that are contributing to the $J_{AF}$ term. As the unpaired electron in V resides in the $d_{xy}$ orbital and the Gd(III) $5d_{z^2}$ and $5_{x^2-y^2}$ orbitals do not lie along with the Gd–V bond, the charge transfer to the Gd(III) 5d orbitals are inefficient here (see Fig. 4b), leading to a weaker $J_F$ term. This leads to a strong antiferromagnetic coupling between the Gd(III) and V(0) spins.

For the **Gd–Mn** complex, the unpaired electron in the Mn atom lies in the $3d_{z^2}$ orbital that is oriented perpendicular to the Gd–Mn bond. This exhibits a much stronger overlap with some of the 4f orbitals, such as $4f_{xyz}$–$3d_{z^2}$ exhibiting a larger overlap than any overlap integral computed for the **Gd–V** complex, rationalising stronger antiferromagnetic coupling observed for this pair (ESI Fig. S2a†). The charge transfer mechanism for **Gd–Mn** follows the same mechanism as that of **Gd–V**, and hence the overall exchange is governed by the orbital overlaps. For the **Gd–Co** pair, the unpaired electron in Co(0) is found in the $d_{x^2-y^2}$ orbital, which not only overlaps weakly with the 4f orbitals (see ESI Fig. S2b and Table S2a†) but also accomplishes efficient charge transfer to the $5d_{x^2-y^2}$ orbital, leading to a dominant $J_F$ term. For the **Gd–Fe$^+$** complex, a weak ferromagnetic exchange is observed. Although the unpaired electron in Fe(I) is found to be in the $d_{z^2}$ orbital similar to that of the Mn case, the Gd–Fe distances are markedly larger (3.002 Å *vs.* 3.457 Å), and this longer and less repulsive ligand field also tilts the $3d_{z^2}$ orbital nearly perpendicular to the **Gd–Fe$^+$** bond leading to a very weak overlap. However, some charge-transfer contributions are retained, leading to weak ferromagnetic coupling.

For the **Gd–V$_{hs}$** complex, the exchange is estimated to be −162.1 cm$^{-1}$ due to several dominant 3d–4f overlaps (see Fig. 5a, S2c and Table S2c in the ESI†).

### Effect of large magnetic exchange in the magnetic anisotropies of the Dy/Er–V, Dy/Er–Mn, Dr/Er–Co complexes

To understand the nature of the magnetic anisotropies of the complexes studied earlier, we modelled two anisotropic metal ions, namely, Dy(III) and Er(III), in place of the Gd(III) ion. To study the single-ion anisotropy of the lanthanide metal ion, the transition metal is replaced by the diamagnetic ions such as Zn(II). Similarly, to study the single-ion anisotropy of the transition metal ion, the diamagnetic Lu(III) ion is used in our model. To gain confidence in the methodology, we begin our study with the [PyCp$_2$DyFeCp(CO)$_2$] (**Dy–Fe**) complex reported by Nippe *et al.*[36] CASSCF/RASSI-SO/SINGLE_ANISO calculations on the X-ray structure of **Dy–Fe** suggest the $m_J = \pm|15/2\rangle$

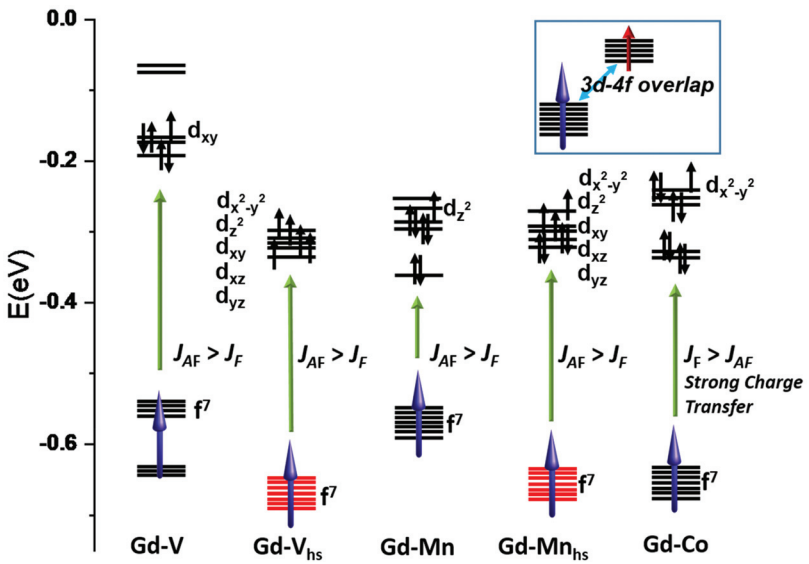


Fig. 5 Mechanism of exchange coupling developed between the overlap of 4f (α-electrons) orbitals of Gd(III) ion and 3d (β-electrons) orbitals of the transition metal ion.

ground state with some mixing with the $m_J$ = ±|11/2⟩ state leading to moderately strong tunnelling at the ground state, suggesting that zero-field SMM is not possible. The first excited state KD was found to lie at 268.7 $cm^{-1}$ with a much stronger TA-QTM (thermally assisted quantum tunneling of magnetisation) probability. However, applying an external magnetic field could quench the ground state QTM leading to a possibility of observing slow relaxation of magnetisation in the presence of applied field conditions. Experimentally, the **Dy–Fe** molecule was found to exhibit field-induced SMM behaviour with the estimated barrier height of 40 $cm^{-1}$. Our calculations rationalise this observation and also reproduce the experimental susceptibility data (see Fig. S7 and S8 in the ESI†), offering confidence in the anisotropic calculations performed.

For the paramagnetic transition metal ion containing complexes, the POLY_ANISO module is used to combine the single-ion magnetic behaviour computed for lanthanide and transition metal ions along with the estimated exchange coupling to derive the magnetic characteristics. For the **Dy–V**, **Dy–Mn** and **Dy–Co** complexes, the low-lying eight KDs show energy distribution in the range of 400–444 $cm^{-1}$ (Table 2) with the increase in CF in accordance with the strength of the Ln–TM bond (Table 1). For **Er–V**, **Er–Mn** and **Er–Co**, on the other hand, overall splitting ranging from 331 $cm^{-1}$ to 351 $cm^{-1}$ is noticed, although they do not reflect the nature of the Ln–TM bond. The ground $g_{zz}$ anisotropy for all the Dy–TM complexes was found to lie along the Cp–Dy–Cp axis (see Fig. 6a), and therefore, the Dy–TM bond lies along the transverse direction obstructing a good SMM behaviour as expected.

On the other hand, for the Er–TM complexes, the $g_{zz}$ axis lies along the Er–TM bond (Fig. 6b), aiding stronger axiality. However, here the Cp rings are hindering the stronger axiality. For this reason, the corresponding ligand field environment is less suitable for the Dy(III) ion compared to the pseudolinear Cp–Dy–Cp* complexes. Furthermore, the Dy–TM bond also enhances the bending of the Cp–Dy–Cp angle leading to a weaker axiality rendered by the Cp rings compared to the [Dy($Cp^{ttt}_2$)][$B(C_6F_5)_4$], with ($Cp^{ttt}$ = $C_5H_2{}^tBu_3$-1,2,4) analogues (145°

**Table 2** CASSCF computed magnetic anisotropy parameters associated with the **Ln–TM** complexes studied. KD energies are given in $cm^{-1}$

| Complexes | V–Dy | Mn–Dy | Co–Dy | V–Er | Mn–Er | Co–Er |
|---|---|---|---|---|---|---|
| KD1 | 0.0 | 0.0 | 0.0 | 0.0 | 0.0 | 0.0 |
| KD2 | 113.5 | 122.2 | 126.2 | 37.5 | 33.5 | 31.3 |
| KD3 | 233.9 | 243.6 | 224.5 | 75.8 | 75.0 | 64.4 |
| KD4 | 262.5 | 274.9 | 249.9 | 153.7 | 162.4 | 158.5 |
| KD5 | 273.0 | 292.8 | 267.5 | 177.6 | 175.9 | 167.3 |
| KD6 | 306.9 | 323.2 | 315.2 | 195.4 | 195.7 | 182.6 |
| KD7 | 347.6 | 366.1 | 374.7 | 263.4 | 262.2 | 248.9 |
| KD8 | 400.7 | 442.9 | 444.6 | 348.4 | 350.9 | 331.5 |
| $g_{xx}$ | 0.013 | 0.008 | 0.003 | 4.791 | 4.048 | 1.409 |
| $g_{yy}$ | 0.024 | 0.014 | 0.007 | 5.054 | 5.140 | 3.972 |
| $g_{zz}$ | 18.975 | 19.033 | 19.124 | 9.368 | 9.760 | 11.299 |
| $g_{xx}$ | 2.018 | 1.407 | 0.601 | 6.930 | 6.514 | 8.258 |
| $g_{yy}$ | 4.399 | 2.787 | 0.658 | 5.165 | 6.191 | 5.065 |
| $g_{zz}$ | 13.503 | 15.748 | 17.854 | 0.925 | 1.234 | 0.861 |

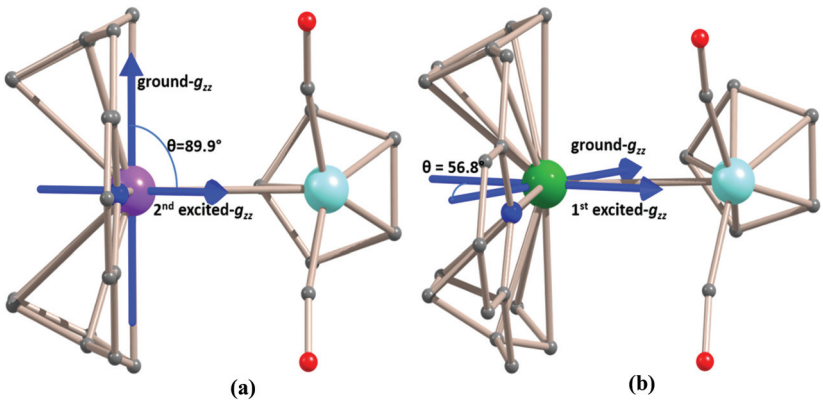


**Fig. 6** Arrangement of ground state and second excited state anisotropy axis for complexes (a) **Dy–V** and (b) **Er–V**.

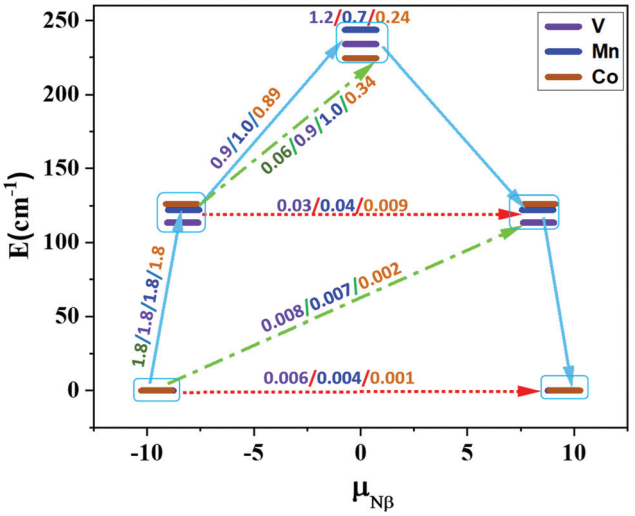


Fig. 7 Dynamics of magnetic relaxation for complexes **Dy–V**, **Dy–Mn** and **Dy–Co** obtained from SINGLE_ANISO calculations. Red dotted line represents QTM, blue solid line represents the TA and green line represents the Raman/Orbach processes. The number on the top of the arrows indicates the mean value of the transition probability between the corresponding states.

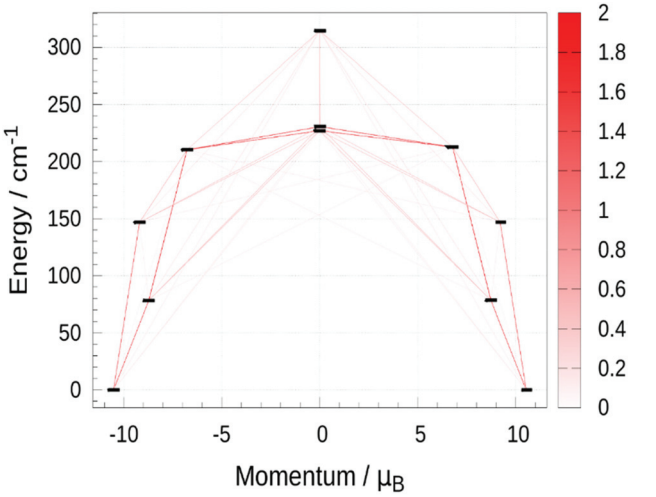


Fig. 8 POLY_ANISO computed magnetic relaxation pathways for the complex **Dy–Co**. Red bar represents the transition probabilities between the corresponding states.

*vs.* 167°, see Table 1). As the ground state anisotropy axis lies along the two Cp rings, strong axiality at the ground state ($g_{zz}$ ~ 19) as well as at the first excited state ($g_{zz}$ ~ 17) are noticed, with the second excited state showing a significant transverse component ($g_{xx/yy}$ ~ 0.65 to 4.39) causing the magnetisation to relax *via* this state. Moreover, the ground state and first excited state $g_{zz}$ axis are almost collinear, but the second excited state $g_{zz}$ lies along the Dy–TM bond with a tilt angle of ~90° (Fig. 6a, b and ESI Fig. S4†). A similar scenario is noted for all the three **Dy–V**, **Dy–Mn**, and **Dy–Co** complexes with a strong TA-QTM or Raman/Orbach process with the first to the second excited state for Dy–M complexes yielding single-ion $U_{cal}$ values of 234 $cm^{-1}$, 244 $cm^{-1}$ and 226 $cm^{-1}$, respectively (see Fig. 7).[70] For the Er(III) ion, a strong transverse component is detected at the ground state, as it has been already established that Cp ligand systems are not suitable for prolate Er(III) ions. For this reason, a strong transverse anisotropy is detected at the ground state leading to strong ground state QTM effects (ESI Fig. S3†).

The *J* value obtained using DFT calculations has been used in the POLY_ANISO module to extract the energy barrier for the exchange-coupled states of the Dy–TM complexes, and these calculations were not performed for the Er analogues as they do not have strong axial anisotropy even at the single-ion level. From the single-ion anisotropy calculations, it was clear that the Dy complexes are showing axial anisotropy in the ground and the first excited state. The combination of such anisotropy with large exchange values is expected to yield a large $U_{eff}$ for the complexes. The developed mechanism of magnetisation relaxation for the Dy–Co is shown in Fig. 8 and in Fig. S5a–c† for other Dy–TM complexes. For the **Dy–V** complex, the estimated $U_{cal}$ value is 187 $cm^{-1}$, and the $\Delta_{tun} < 10^{-9}$ $cm^{-1}$ suggests complete annihilation of the QTM behaviour from the ground state to the fourth excited state due to strong exchange coupling. However, the $U_{cal}$ value for this complex is 49 $cm^{-1}$ smaller than the single-ion anisotropy due to the antiferromagnetic **Gd–V** exchange that destabilises the $m_J \pm\frac{1}{2}$ level in the exchange-coupled mechanism compared to the corresponding single-ion levels. While this is expected to reduce the $U_{cal}$ value, this is likely to be more than compensated by the quenching of QTM due to the presence of strong exchange coupling, which is harder to fine-tune compared to the $U_{cal}$ values. For the **Dy–Mn** complex, also a similar picture emerges with the estimated $U_{eff}$ value of 218 $cm^{-1}$ which is 26 $cm^{-1}$ lower than the corresponding single-ion derived $U_{cal}$ value. For the **Dy–Co** complex, this value has increased to 229 $cm^{-1}$, which is more than the single-ion calculated $U_{cal}$ value, and presents the best case among the complexes studied. For the high spin analogues of V and Mn, the $U_{cal}$ values obtained are 86 $cm^{-1}$ and 174 $cm^{-1}$, respectively, and this is due to their large antiferromagnetic interaction stabilising the lowest $m_J$ states. In all the cases, it has been observed that the QTM is completely suppressed ($\Delta_{tun} < 10^{-10}$ $cm^{-1}$) due to the large exchange coupling and the relaxation mechanism is arising due to the Raman/Orbach processes.

## Conclusions

In this work, we have conducted detailed DFT and CASSCF studies on 3d–4f complexes possessing unsupported Ln–TM direct bonds as a way to fine-tune magnetic exchange interactions. Conclusions derived from this work are summarised below:

(i) ***Structure and bonding in complexes containing Ln–TM direct bonds***: We have modelled using DFT [$PyCp_2GdMCp(CO)_2$] (M = V, Mn, Co, and $Fe^+$) complexes and probed the Ln–Tm bonds using CASSCF computed AILFT and NBO analyses. Our calculations suggest a dative Ln–TM bond with a donation

of $\pi$(V/Mn$d_{xy}$–$\pi^*$CO) to 5$d_{z^2}$ (Gd) in the case of Gd–V and Gd–Mn and 4s(Co) to 5$d_{xy}$/5$d_{yz}$ (Gd) for Gd–Co is detected. Bond order calculations reveal that the strength of the bonds is similar to that of the $NH_3 \rightarrow BH_3$ donor–acceptor bonds. The AILFT analysis reveals that all the transition metal ions are in the low-spin configuration due to strong donations from the CO and Cp ligands, with the excited high-spin configurations predicted to be hundreds of kJ mol$^{-1}$ higher.

(ii) ***Record high ferro-antiferro exchange coupling via Gd–TM bonds***: DFT calculations yield the following $J$ values: $J_{Gd-V}$ = −46.1 cm$^{-1}$, $J_{Gd-Mn}$ = −57.1, $J_{Gd-Co}$ = +55.3 cm$^{-1}$ $J_{Gd-Fe^+}$ = +13.9 cm$^{-1}$ $J_{Gd-V_{hs}}$ = −162.1 cm$^{-1}$ and $J_{Gd-Mn_{hs}}$ = −343.9 cm$^{-1}$. All these {3d–4f} $J$ values are at least an order of magnitude larger than the values known for conventional {3d–4f} complexes and some of the $J$ values are record high-values for any radical/{3d–4f} complexes reported suggesting a viable way to enhance a key parameter that remain elusive.

(iii) ***Direct-exchange {3d–4f} interaction mechanism established***: Similar to the super-exchange mechanism developed for {3d–4f} pairs, there are ferro and antiferromagnetic contributions to the net exchange. The difference here is that both contributions are significantly larger and the dominant contribution (so is the sign) is decided by the electronic configuration of the transition metal ions. Unlike conventional {3d–4f} complexes, here, the 3d–4f SOMO overlaps are dominant, leading to antiferromagnetic coupling in most of the cases studied. When such overlaps are weaker, and the Gd(5$d_{z^2}$) orbital lies along the Ln–TM bond, the charge transfer dominates and leads to a net ferromagnetic interaction. If the number of unpaired electrons on the transition metal centre increases, this increases the 3d–4f SOMO overlaps, leading to an extremely large antiferromagnetic coupling, as witnessed in some of the systems studied.

(iv) ***Record-high barrier height for magnetization reversal for {3d–4f} complexes***: We have modelled the analogue Dy(III) and Er(III) complexes to probe the magnetic anisotropy and the role of exchange coupling in suppressing the associated QTM behaviour. Our calculations reveal that the Ln–TM bond hinders the axial anisotropy in the case of Dy(III) as it lies perpendicular to the ground state $g_{zz}$ axis. For Er(III) ions, though it helps it is not significant enough to yield superior SMM behaviour. The incorporation of exchange coupling negate these negative effects and offers record-high barrier height for magnetisation reversal for systems when a ferromagnetic coupling is present. This unveils a hitherto unknown strategy to fine-tune magnetisation reversal barrier in {3d–4f} complexes.

To this end, using a combination of theoretical tools, we have studied the role of Ln–TM bonds in estimating the direct exchange and its influence on the magnetisation reversal barrier. Encouraging results are obtained in some of the systems studied, suggesting a lanthanide–transition metal bond as a design strategy to unveil new generation SMMs.

## Conflicts of interest

The authors have no conflict of interest.

## Acknowledgements

We thank DST and SERB (CRG/2018/00430; DST/CSA-03/2018-10; and SB/SJF/2019-20/12) for funding. AbS/AS thanks UGC/CSIR for a fellowship.

## References

1 G. Christou, D. Gatteschi, D. N. Hendrickson and R. Sessoli, *MRS Bull.*, 2000, **25**, 66–71.
2 R. Sessoli, D. Gatteschi, A. Caneschi and M. Novak, *Nature*, 1993, **365**, 141–143.
3 L. Bogani and W. Wernsdorfer, in *Nanoscience and technology: a collection of reviews from nature journals*, World Scientific, 2010, pp. 194–201.
4 G. Aromí, D. Aguila, P. Gamez, F. Luis and O. Roubeau, *Chem. Soc. Rev.*, 2012, **41**, 537–546.
5 A. Ardavan, O. Rival, J. J. Morton, S. J. Blundell, A. M. Tyryshkin, G. A. Timco and R. E. Winpenny, *Phys. Rev. Lett.*, 2007, **98**, 057201.
6 M. Affronte, F. Troiani, A. Ghirri, A. Candini, M. Evangelisti, V. Corradini, S. Carretta, P. Santini, G. Amoretti and F. Tuna, *J. Phys. D: Appl. Phys.*, 2007, **40**, 2999–3004.
7 T. Gupta and G. Rajaraman, *Chem. Commun.*, 2016, **52**, 8972–9008.
8 D. N. Woodruff, R. E. Winpenny and R. A. Layfield, *Chem. Rev.*, 2013, **113**, 5110–5148.
9 D. Gatteschi and R. Sessoli, *Angew. Chem., Int. Ed.*, 2003, **42**, 268–297.
10 C. A. Goodwin, F. Ortu, D. Reta, N. F. Chilton and D. P. Mills, *Nature*, 2017, **548**, 439–442.
11 F.-S. Guo, B. M. Day, Y.-C. Chen, M.-L. Tong, A. Mansikkamäki and R. A. Layfield, *Science*, 2018, **362**, 1400–1403.
12 R. J. Blagg, L. Ungur, F. Tuna, J. Speak, P. Comar, D. Collison, W. Wernsdorfer, E. J. McInnes, L. F. Chibotaru and R. E. Winpenny, *Nat. Chem.*, 2013, **5**, 673–678.
13 J. D. Rinehart, M. Fang, W. J. Evans and J. R. Long, *Nat. Chem.*, 2011, **3**, 538–542.
14 P. P. Hallmen, H.-J. Werner, D. Kats, S. Lenz, G. Rauhut, H. Stoll and J. van Slageren, *Phys. Chem. Chem. Phys.*, 2019, **21**, 9769–9778.
15 S. Liu, L. Gelmini, S. J. Rettig, R. C. Thompson and C. Orvig, *J. Am. Chem. Soc.*, 1992, **114**, 6081–6087.
16 S. A. Sulway, R. A. Layfield, F. Tuna, W. Wernsdorfer and R. E. Winpenny, *Chem. Commun.*, 2012, **48**, 1508–1510.
17 H. Tian, L. Ungur, L. Zhao, S. Ding, J. Tang and L. F. Chibotaru, *Chemistry*, 2018, **24**, 9928–9939.
18 L. Zhong, W.-B. Chen, X.-H. Li, Z.-J. OuYang, M. Yang, Y.-Q. Zhang, S. Gao and W. Dong, *Inorg. Chem.*, 2020, **59**, 4414–4423.
19 S. Dey and G. Rajaraman, *Dalton Trans.*, 2020, **49**, 14781–14785.

 

20 J. D. Rinehart, M. Fang, W. J. Evans and J. R. Long, *J. Am. Chem. Soc.*, 2011, **133**, 14236–14239.
21 T. Rajeshkumar and G. Rajaraman, *Chem. Commun.*, 2012, **48**, 7856–7858.
22 L. E. Darago, M. D. Boshart, B. D. Nguyen, E. Perlt, J. W. Ziller, W. W. Lukens, F. Furche, W. J. Evans and J. R. Long, *J. Am. Chem. Soc.*, 2021, 8465–8475.
23 S. K. Langley, D. P. Wielechowski, V. Vieru, N. F. Chilton, B. Moubaraki, L. F. Chibotaru and K. S. Murray, *Chem. Commun.*, 2015, **51**, 2044–2047.
24 Y. Peng and A. K. Powell, *Coord. Chem. Rev.*, 2021, **426**, 213490.
25 G. Velkos, D. S. Krylov, K. Kirkpatrick, L. Spree, V. Dubrovin, B. Büchner, S. M. Avdoshenko, V. Bezmelnitsyn, S. Davis and P. Faust, *Angew. Chem., Int. Ed.*, 2019, **58**, 5891–5896.
26 M. K. Singh, N. Yadav and G. Rajaraman, *Chem. Commun.*, 2015, **51**, 17732–17735.
27 J.-L. Liu, J.-Y. Wu, G.-Z. Huang, Y.-C. Chen, J.-H. Jia, L. Ungur, L. F. Chibotaru, X.-M. Chen and M.-L. Tong, *Sci. Rep.*, 2015, **5**, 1–9.
28 T. Rajeshkumar, R. Jose, P. R. Remya and G. Rajaraman, *Inorg. Chem.*, 2019, **58**, 11927–11940.
29 T. Gupta, T. Rajeshkumar and G. Rajaraman, *Phys. Chem. Chem. Phys.*, 2014, **16**, 14568–14577.
30 S. K. Singh and G. Rajaraman, *Dalton Trans.*, 2013, **42**, 3623–3630.
31 I. Beletskaya, A. Voskoboynikov, E. Chuklanova, N. Kirillova, A. Shestakova, I. Parshina, A. Gusev and G. Magomedov, *J. Am. Chem. Soc.*, 1993, **115**, 3156–3166.
32 P. L. Arnold, J. McMaster and S. T. Liddle, *Chem. Commun.*, 2009, 818–820.
33 M. V. Butovskii, O. L. Tok, V. Bezugly, F. R. Wagner and R. Kempe, *Angew. Chem., Int. Ed.*, 2011, **50**, 7695–7698.
34 C. Döring, A. M. Dietel, M. V. Butovskii, V. Bezugly, F. R. Wagner and R. Kempe, *Chem. – Eur. J.*, 2010, **16**, 10679–10683.
35 M. e. V. Butovskii, O. e. L. Tok, F. e. R. Wagner and R. Kempe, *Angew. Chem., Int. Ed.*, 2008, **47**, 6469–6472.
36 C. P. Burns, X. Yang, J. D. Wofford, N. S. Bhuvanesh, M. B. Hall and M. Nippe, *Angew. Chem., Int. Ed.*, 2018, **57**, 8144–8148.
37 D. Fritsch, K. Koepernik, M. Richter and H. Eschrig, *J. Comput. Chem.*, 2008, **29**, 2210–2219.
38 A. V. Postnikov, J. Kortus and M. R. Pederson, *Phys. Status Solidi B*, 2006, **243**, 2533–2572.
39 K. Yamaguchi, S. Yamanaka, M. Nishino, Y. Takano, Y. Kitagawa, H. Nagao and Y. Yoshioka, *Theor. Chem. Acc.*, 1999, **102**, 328–345.
40 M. Frisch, G. Trucks, H. Schlegel, G. Scuseria, M. Robb, J. Cheeseman, G. Scalmani, V. Barone, G. Petersson and H. Nakatsuji, Gaussian, Inc., Wallingford CT, 2016, https://gaussian.com/citation/.
41 L. Chengteh, Y. Weitao and R. Parr, *Phys. Rev. B: Condens. Matter Mater. Phys.*, 1988, **37**, 785–789.
42 A. D. Becke, *Phys. Rev. A*, 1988, **38**, 3098.
43 T. R. Cundari and W. J. Stevens, *J. Chem. Phys.*, 1993, **98**, 5555–5565.
44 T. H. Dunning and P. J. Hay, *Mod. Theor. Chem.*, 1977, **3**, 1–28.
45 K. Eichkorn, F. Weigend, O. Treutler and R. Ahlrichs, *Theor. Chem. Acc.*, 1997, **97**, 119–124.
46 T. Kawakami, K. Miyagawa, H. Isobe, M. Shoji, S. Yamanaka, M. Katouda, T. Nakajima, K. Nakatani, M. Okumura and K. Yamaguchi, *Chem. Phys. Lett.*, 2018, **705**, 85–91.
47 F. Neese, F. Wennmohs, U. Becker and C. Riplinger, *J. Chem. Phys.*, 2020, **152**, 224108.
48 S. K. Singh, J. Eng, M. Atanasov and F. Neese, *Coord. Chem. Rev.*, 2017, **344**, 2–25.
49 F. Aquilante, J. Autschbach, R. K. Carlson, L. F. Chibotaru, M. G. Delcey, L. De Vico, I. F. Galván, N. Ferré, L. M. Frutos and L. Gagliardi, *J. Comp. Chem.*, 2016, 506–541.
50 L. Chibotaru and L. Ungur, University of Leuven, 2006, https://chem.kuleuven.be/en/research/qcpc/ton/software-1.
51 L. Chibotaru and L. Ungur, *Ungur, LF Chibotaru in* http://www.molcas.org/documentation/manual/node105.html.
52 L. F. Chibotaru and L. Ungur, *J. Chem. Phys.*, 2012, **137**, 064112.
53 L. F. Chibotaru, L. Ungur, C. Aronica, H. Elmoll, G. Pilet and D. Luneau, *J. Am. Chem. Soc.*, 2008, **130**, 12445–12455.
54 L. F. Chibotaru, L. Ungur and A. Soncini, *Angew. Chem.*, 2008, **120**, 4194–4197.
55 T. Gupta, M. K. Singh and G. Rajaraman, in *Organometallic Magnets*, Springer, 2018, pp. 281–354.
56 M. Douglas and N. M. Kroll, *Ann. Phys.*, 1974, **82**, 89–155.
57 E. D. Glendening, C. R. Landis and F. Weinhold, *J. Comput. Chem.*, 2013, **34**, 1429–1437.
58 L. Noodleman, *J. Chem. Phys.*, 1981, **74**, 5737–5743.
59 S. Sinnecker, F. Neese, L. Noodleman and W. Lubitz, *J. Am. Chem. Soc.*, 2004, **126**, 2613–2622.
60 L. Noodleman, D. A. Case and A. Aizman, *J. Am. Chem. Soc.*, 1988, **110**, 1001–1005.
61 E. Ruiz, J. Cano, S. Alvarez and P. Alemany, *J. Comput. Chem.*, 1999, **20**, 1391–1400.
62 E. Ruiz, A. Rodríguez-Fortea, J. Cano, S. Alvarez and P. Alemany, *J. Comput. Chem.*, 2003, **24**, 982–989.
63 T. Yamasaki and W. A. Goddard, *J. Phys. Chem. A*, 1998, **102**, 2919–2933.
64 X. Yang, C. P. Burns, M. Nippe and M. B. Hall, *Inorg. Chem.*, 2021, 9394–9401.
65 B. N. Figgis and M. A. Hitchman, *Ligand field theory and its applications*, Wiley-Vch, New York, 2000.
66 S. K. Singh, M. Atanasov and F. Neese, *J. Chem. Theory Comput.*, 2018, **14**, 4662–4677.
67 G. Rajaraman, F. Totti, A. Bencini, A. Caneschi, R. Sessoli and D. Gatteschi, *Dalton Trans.*, 2009, 3153–3161.
68 J. Paulovič, F. Cimpoesu, M. Ferbinteanu and K. Hirao, *J. Am. Chem. Soc.*, 2004, **126**, 3321–3331.
69 R. Carrasco, I. Morgenstern-Badarau and J. Cano, *Chem. Commun.*, 2003, 436–437.
70 A. Abragam and B. Bleaney, *Electron paramagnetic resonance of transition ions*, OUP, Oxford, 2012.